Nonlinear ferromagnetic resonance shift in submicron Permalloy ellipses

Feng Guo, Lyubov M. Belova, and Robert D. McMichael

Phys. Rev. B **91**, 064426 — Published 27 February 2015

DOI: 10.1103/PhysRevB.91.064426

Nonlinear ferromagnetic resonance shift in submicron ellipses

Feng Guo,[1,2,*] Lyubov M. Belova,[3] and Robert D. McMichael[1,†]

[1]*Center for Nanoscale Science and Technology, National Institute of Standards and Technology, Gaithersburg, Maryland 20899, USA*

[2]*Maryland Nanocenter, University of Maryland, College Park, Maryland 20742, USA*

[3]*Department of Materials Science and Engineering, Royal Institute of Technology, 10044 Stockholm, Sweden*

Abstract

We report a systematic study of nonlinearity in the ferromagnetic resonance of a series of submicron Permalloy ellipses with varying aspect ratios. At high excitation powers, the resonances are found to shift to higher or lower applied field. We focus here on the sign of the shift and its dependence on the applied field and shape-induced anisotropy of the ellipses. Using ferromagnetic resonance force microscopy, we find that the measured nonlinear coefficient changes sign as a function of anisotropy field and applied field in qualitative agreement with a macro-spin analysis. This macro-spin analysis also points to origins of the nonlinearity in a combination of hard-axis in-plane anisotropy and precession ellipticity. In comparison of the macro-spin predictions with both experimental and micromagnetic modeling results, we measure/model values of the nonlinear coefficient that are more positive than predicted by the macrospin model. The results are useful in understanding nonlinear physics in nanomagnets and applications of spin-torque oscillators.

From the basic phenomena of hysteresis and switching to the development of modern magnetic memory chips, the nonlinear behavior of ferromagnetism has been a key property that makes magnets useful. Even in conceptually simple experiments involving only a magnet, a static magnetic field, and a relatively small transverse oscillating field to drive dynamics, there is a long and rich history of nonlinear magnetic phenomena[1–3] that includes premature saturation of magnetic resonance, spin wave instabilities,[4] auto-oscillations,[5] chaos, solitons, and even Bose-Einstein condensation of excited magnons.[6]

Perhaps the simplest nonlinear effect is a dependence of the free oscillation frequency, ω_0, on the oscillation amplitude:

$$\omega_0 = \omega_0^{\text{lin}} + N|c|^2, \tag{1}$$

were c is a dynamical variable describing the amplitude and phase of the oscillator, ω_0^{lin} is the low-amplitude resonance frequency and N is the nonlinear frequency shift coefficient. This change in resonant frequency with amplitude leads to a foldover phenomenon where the frequency response of a resonator changes from a symmetric Lorentzian peak at low excitation to an asymmetric peak shape at high excitation, possibly also exhibiting instabilities. The foldover phenomenon is quite general, and it has been studied in systems ranging from pendulums to on-chip optical resonators.

In this study, we focus on the sign of the nonlinear coefficient of the ferromagnetic resonance in submicron magnetic structures where the strong confinement creates discrete spectra of standing spin wave modes. The power dependent ferromagnetic resonance is illustrated in Fig. 1 where the resonance response of a submicron ellipse is plotted for several values of pumping intensity and for two values of pumping frequency. For low excitation power, both resonance curves are nearly symmetric. However, at higher excitation powers, the resonance curves "lean" in opposite directions, indicating that the nonlinear coefficient changes sign. In earlier works, positive[7–10] and negative[10,11] values for the nonlinear coefficient have been reported in a variety of experimental configurations. The changing sign of the nonlinear coefficient has been theoretically explained by Slavin and Tiberkevich using a classical Hamiltonian approach for the dynamics of a macrospin.[12,13] Using a Holstein-Primakoff transformation and a Bogoluibov transformation, the dynamics of the macrospin is described by a pair of canonical variables through the Hamiltonian formalism. A key feature of their result is that the nonlinear coefficient can change sign with increasing applied

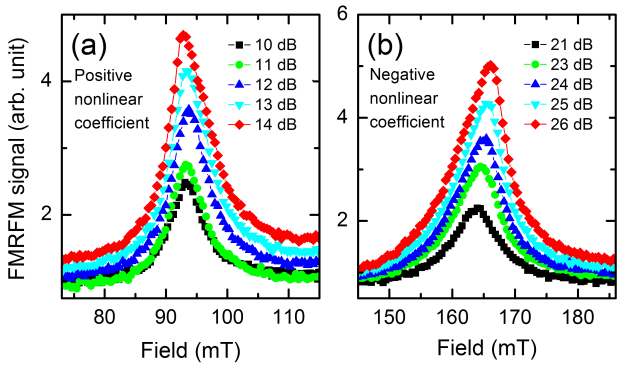

FIG. 1: (Color online) Power dependent resonance spectra measured with a 560 nm × 450 nm elliptical sample with an aspect ratio of 1.25 and with microwave frequencies of (a) 9 GHz and (b) 12 GHz. The static field is applied in plane along the long axis and the microwave field is in plane, perpendicular to the static field.

field when the magnetization is directed along an anisotropy hard axis.

In this paper we confirm both via experiment and via micromagnetic modeling that the nonlinear coefficient changes sign with both the applied field and also the effective shape anisotropy of the nanostructure. We provide a simple derivation of the nonlinear coefficient, and we show the nonlinear resonance shift is determined by a combination of the anisotropy fields and the applied field through the ellipticity of the precession orbit. Finally, we discuss an additional significant resonance shift due to the non-uniformity of the precession mode in confined structures.

The samples used in this study have a trilayer structure of Ta (5 nm)/$Ni_{80}Fe_{20}$ (25 nm)/Ta (5 nm). They are patterned into elliptical shapes using e-beam lithography, e-beam evaporation and a lift-off process. The samples are deposited on a 150 nm thick and 2 μm wide gold waveguide which generates the microwave-frequency pumping field for the resonance measurements. The ellipses are made with in-plane length/width aspect ratios (AR) ranging from 0.5 to 2.0, designed to have areas equivalent to a 500 nm diameter disk.

The spectra are measured using ferromagnetic resonance force microscopy (FMRFM)[14–20], which has a number of advantages for these measurements. First, FMRFM has the ability to measure single structures. By measuring a single structure, we avoid ensemble averaging and we avoid inhomogeneous broadening of the resonances, which would obscure the small resonance shifts. Also, because electrical contacts are not needed, sample fabrication is

simplified, and our measurement focus is easily moved between structures.

In our FMRFM measurements, samples are magnetized in-plane and a nearby cantilever with a 200 nm diameter cobalt probe tip[21] deflects in response to magnetostatic forces between the tip and sample. Precession in the sample is excited by an in-plane microwave driving field via a coplanar waveguide. In the absence of heating, the magnetization vector magnitude remains unchanged in these experiments, so when the precession is large, tip-sample forces are reduced as the time-averaged magnetization is slightly diminished. For maximum cantilever sensitivity, we modulate the microwave power (and therefore also the tip sample forces) at the mechanical resonance frequency of the cantilever. Unfortunately, power modulation prevents us from observing bistable foldover effects, but in this work we focus only on the initial indications of nonlinearity.

Microwave power levels in this paper are given in decibels relative to 1 mW (i.e. in dBm) measured at the output of our signal generator. The microwave power levels at the sample are uncalibrated, but transmission to the sample is known to be both lossy and frequency-dependent.

First we demonstrate the power dependent resonance shift. Fig. 1(a) shows the spectra measured under various microwave powers with a fixed frequency of 9 GHz. At low powers (less than 12 dB), the resonance shows a Lorentzian peak at 93.5 mT. As the power increases the resonance becomes nonlinear: the resonance peak is no longer symmetric and leans towards low-field direction. Furthermore, the resonance field depends on the microwave power. At 9 GHz, the resonance field shifts toward low-field direction ($H_{res} = 92.7$ mT at 14 dB). Similiar power dependent behaviors are observed at 12 GHz, as shown in Fig. 1(b). Asymmetric spectra at high powers indicate nonlinear response. However, in contrast to the 9 GHz spectra, the nonlinear coefficient has a different sign: the resonance field of the 12 GHz spectra increases with power. The power dependent resonance field measurement was repeated from 7 GHz ($H_{res} = 54.5$ mT) to 13 GHz ($H_{res} = 191.5$ mT). In the nonlinear regime, we found that the resonance shifts toward low-field when $f \leq 9$ GHz ($H_{res} \leq 92.8$ mT), while the resonance shifts toward high-field when $f \geq 11$ GHz ($H_{res} \geq 139.2$ mT).

Consistent with Eq. (1), we define positive values of the nonlinear frequency coefficient for resonances peaks that "fold over", leaning toward low fields and negative values for resonance peaks that lean toward high fields. If this definition seems counter-intuitive, note that an increased intrinsic resonance frequency will require a lower applied field to be in

resonance with the driving field. We point out that the field dependence of the nonlinear coefficient shown in Fig. 1 is true for all the samples measured: the nonlinear coefficient is positive (negative) at low (high) fields.

The nonlinear coefficient of a macrospin can be obtained via either a classical Hamiltonian formalism[12,13] or the equation of motion approach. To build in intuition, we derive the nonlinear coefficient directly from the equation of motion which allows us to easily describe the mechanisms of the nonlinearity. We begin with a free energy expression for the macrospin:

$$\frac{E}{\mu_0} = -M_z H_{\text{appl}} + \frac{H_1}{2M_\text{s}} M_x^2 + \frac{H_2}{2M_\text{s}} M_y^2, \tag{2}$$

where μ_0 is the permeability of vacuum, H_{appl} is the external field applied along the z-direction. Effective anisotropy fields H_1 and H_2 include the effects of magnetostatic interactions and exchange. We take the film normal to be parallel to the y-direction, so H_2 will be large and positive, owing to the thin film character of our samples. The in-plane anisotropy, H_1, due to the lithographically defined shapes, will generally be much smaller.

We start with the Landau-Lifshitz equations of motion neglecting the damping, $d\mathbf{M}/dt = -\mu_0\gamma \mathbf{M} \times \mathbf{H}_{\text{eff}}$ (γ is the gyromagnetic ratio), and convert it to the spherical coordinates with $M_x = M_\text{s} \sin\theta \cos\phi$, $M_y = M_\text{s} \sin\theta \sin\phi$, and $M_z = M_\text{s} \cos\theta$, where θ is the polar angle and ϕ is the azimuthal angle. In the spherical coordinate system, the equation of motion for the azimuthal angle is

$$\frac{d\phi}{dt} = \frac{\gamma}{M_\text{s} \sin\theta} \frac{\partial E}{\partial \theta}. \tag{3}$$

To lowest order in the precession cone angle θ,

$$\begin{aligned} \frac{d\phi}{dt} \;&=\; \mu_0\gamma(H_{\text{appl}} + H_1 \cos^2\phi + H_2 \sin^2\phi) \\ &\quad -\frac{\mu_0\gamma\theta^2}{2}(H_1 \cos^2\phi + H_2 \sin^2\phi). \end{aligned} \tag{4}$$

In this expression, the second term explicitly describes the nonlinearity that comes from expansion of $E(\theta, \phi)$ around the energy minimum to include non-quadratic terms.

The conservation of energy during precession dictates the relationship between θ and ϕ. For an energy $E = E_0 + \Delta E$ slightly above the energy minimum, $E_0 = -\mu_0 M_\text{s} H_{\text{appl}}$,

$$\theta^2 = \frac{2\Delta E}{\mu_0 M_\text{s}} (H_{\text{appl}} + H_1 \cos^2\phi + H_2 \sin^2\phi)^{-1}. \tag{5}$$

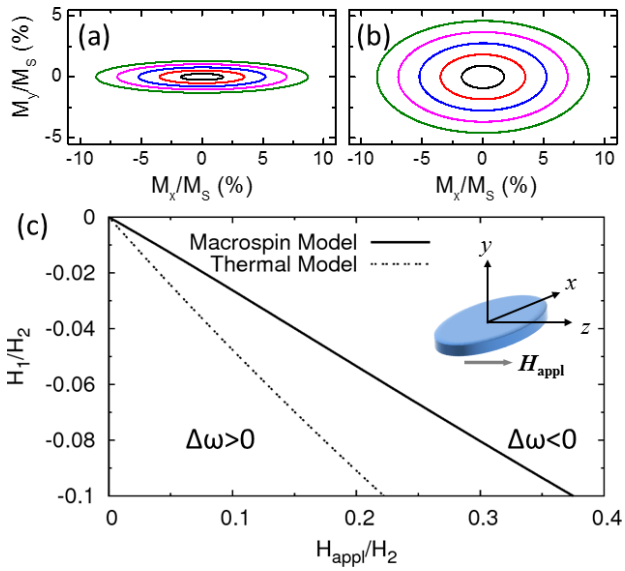

FIG. 2: (Color online) Calculated precession orbits projected in the x-y plane with an applied field of (a) $H_{\rm appl}/H_2 = 0.10$ and (b) $H_{\rm appl}/H_2 = 0.49$. For both (a) and (b), $H_1/H_2 = -0.07$. Different trajectories correspond to $\theta_x = 1°, 2°, 3°, 4°$, and $5°$, where θ_x is the polar angle as the magnetization sweeps through the x-z plane, i.e., $\theta_x = \sin^{-1}(M_x^{\rm max}/M_s)$. (c) Zero nonlinear coefficient curves predicted by the macrospin model, Eq. (8, solid line) and thermal nonlinearity, Eq. (11), dashed line).

The precession period T is found by inverting and integrating (4). Keeping only lowest-order terms in θ, we get:

$$T = \frac{1}{\mu_0\gamma}\int_0^{2\pi}\frac{d\phi}{H_{\rm appl}+H_1\cos^2\phi+H_2\sin^2\phi} + \frac{\Delta E}{\mu_0^2\gamma M_{\rm s}}\int_0^{2\pi}\frac{d\phi\ (H_1\cos^2\phi+H_2\sin^2\phi)}{(H_{\rm appl}+H_1\cos^2\phi+H_2\sin^2\phi)^3}+\ldots. \tag{6}$$

The integrals in Eq. (6) can be performed, and after inverting the period we obtain the angular precession frequency: $\omega = \omega_0 + \Delta\omega$ where

$$\omega_0 = \mu_0\gamma\sqrt{(H_{\rm appl}+H_1)(H_{\rm appl}+H_2)} \tag{7}$$

is the linear frequency for small precession amplitudes, and

$$\Delta\omega = -\frac{\mu_0^3\gamma^4\Delta E}{2M_{\rm s}\omega_0^3}[(H_1+H_2)(\frac{\omega_0}{\mu_0\gamma})^2-\frac{3}{4}H_{\rm appl}(H_1-H_2)^2] \tag{8}$$

is the nonlinear frequency shift. Eq. (8) presents a result consistent with the analysis developed by Slavin and Tiberkevich.[12] We point out that the macro-spin analysis yields a

general result that only depends on the strength of the anisotropy fields and the applied field, rather than the particular origins of the anisotropy.

For many thin-film sample shapes, H_2 is large and positive, and it would seem from (4) that the nonlinear term would generally tend to slow precession, i.e. the nonlinear coefficient should be negative. If both H_1 and H_2 are positive, as when the magnetization aligns along easy axis, the right hand side of (4) is positive, so the precession slows down and $\Delta\omega < 0$.

However, when the magnetization lies in the in-plane hard axis direction, $H_1 < 0$ and $H_2 > 0$, and the in-plane and out-of-plane anisotropy terms have oppositely signed contributions to the nonlinearity. Although $|H_2| > |H_1|$, the H_2 term is not necessarily dominant because the ellipticity of the precession results in unequal sampling of H_1 and H_2. At low fields, the precession orbit is highly elliptical. The precession amplitude in the x direction is much larger than that in the y direction, thus the H_1 term is more important in determining the nonlinearity and $\Delta\omega > 0$. However, at higher fields, the precession orbit becomes more circular which means H_1 and H_2 are sampled more equally. The H_2 term quickly becomes dominant and $\Delta\omega < 0$.

The boundary between positive and negative nonlinearity predicted by (8) is plotted in Fig. 2(c) in terms of the in-plane anisotropy field and applied field. It is clear from this plot that the nonlinear coefficient is expected to change sign as a function of $H_{\rm appl}$ when H_1 is negative.

So far, we have considered only nonlinear mechanisms that arise from precession dynamics, but thermal mechanisms may also drive nonlinear effects. Here, we briefly consider a macrospin model for thermal nonlinearity.

Additional microwave power that is absorbed and dissipated at resonance can be expected to produce a temperature rise δT along with reductions in both the saturation magnetization $\delta M_{\rm s} = (dM_{\rm s}/dT)\delta T$ and also similarly in the exchange stiffness A. To estimate the behavior of the thermal nonlinearity, we recast (7) in terms of shape anisotropies and exchange fields.

$$H_1 \;=\; (N_x - N_z)M_{\rm s} + H_{\rm ex} \tag{9}$$

$$H_2 \;=\; (N_y - N_z)M_{\rm s} + H_{\rm ex} \tag{10}$$

where N_x, N_y and N_z are effective shape demagnetization factors and $H_{\rm ex} \propto 2A/M_{\rm s}$. We relate thermal changes $H_{\rm ex}$ to changes in $M_{\rm s}$, by assuming that the magnetization and the exchange stiffness follow a scaling relation, $A \propto M_{\rm s}^{\beta}$. Using these assumptions, we find

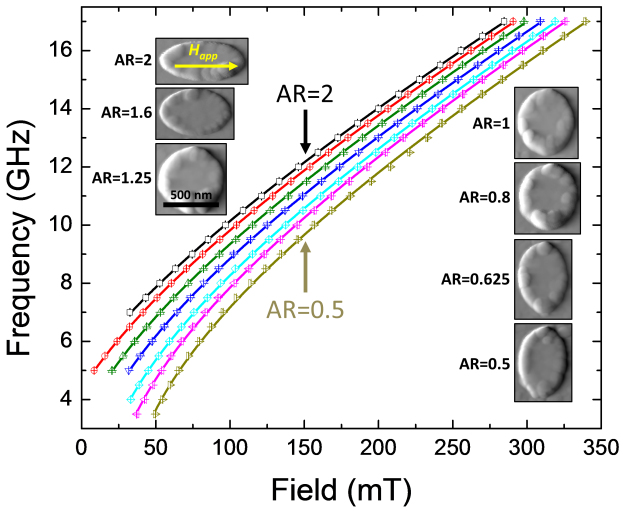

FIG. 3: (Color online) Frequency as a function of applied field measured in linear regime for elliptical samples with various aspect ratios. The microwave power here is typically one order of magnitude less than in the nonlinear measurements (e.g. fig. 1). The symbols represent experimental data and the solid lines are the fits using the Kittel equation. The insets are the AFM images using the same 200 nm probe.

the zero-nonlinearity boundary between thermally-induced magnetization shifts by asserting that a small change in M_s will produce no shift in the resonant frequency, eq. (7). Taking the derivative of (7) with respect to M_s and setting the result to zero yields the estimated boundary between positive and negative frequency shift by a thermal mechanism:

$$\frac{H_1}{H_2} = -\frac{\frac{H_{\rm appl}}{H_2}\left[1+2(\beta-2)\frac{H_{\rm ex}}{H_2}\right]+(\beta-2)\frac{H_{\rm ex}}{H_2}}{2+\frac{H_{\rm appl}}{H_2}+(\beta-2)\frac{H_{\rm ex}}{H_2}} \tag{11}$$

Note that if the exchange stiffness scales as the square of the magnetization ($\beta = 2$), as is often assumed, the exchange fields do not play a role. The boundary given by (11) is plotted for $\beta = 2$ as a dashed line in Fig. 2(c). Although the thermal mechanism and the dynamic mechanisms both exhibit the same overall trend, i.e. changing from positive to negative with increasing applied field, the zero-crossing condition is quite different for the two mechanisms.

We now present our measurements of the sign of the nonlinear coefficient as a function of applied field and anisotropy field. We utilize the shape anisotropy to vary the in-plane anisotropy field. A series of 7 elliptical samples with the same area but different aspect ratios (AR) are fabricated for this experiment.

TABLE I: Measured and modeled values of in-plane anisotropy field, H_1, and effective out-of-plane anisotropy, H_2, for the elliptical samples. The values were determined by fitting low power resonance fields to the Kittel FMR equation, eq. (7). Uncertainties are the standard deviations of the fit parameters.

	Measurement		Modeling	
Sample	$\mu_0 H_1$ (mT)	$\mu_0 H_2$ (mT)	$\mu_0 H_1$ (mT)	$\mu_0 H_2$ (mT)
AR=0.5	-31.3 ± 0.4	853 ± 4	-44.9 ± 0.2	909 ± 2
AR=0.625	-19.6 ± 0.2	877 ± 2	-30.5 ± 0.2	910 ± 2
AR=0.8	-10.2 ± 0.2	870 ± 2	-14.5 ± 0.2	902 ± 1
AR=1	3.2 ± 0.2	867 ± 2	0.3 ± 0.1	908.4 ± 0.6
AR=1.25	14.8 ± 0.3	870 ± 2	15.15 ± 0.06	903.5 ± 0.3
AR=1.6	27.9 ± 0.1	861 ± 1	30.80 ± 0.04	901.3 ± 0.2
AR=2	36.6 ± 0.3	862 ± 2	46.19 ± 0.05	897.5 ± 0.2

In order to characterize the anisotropy fields of these samples, FMR resonances are first measured at low microwave powers as shown in Fig. 3. For each sample, the FMR curve is fitted using the Kittel equation, Eq. (7), with two fitting parameters H_1, the in-plane anisotropy field (or the saturation field), and H_2, the out of plane anisotropy field. The best-fit values of H_1 and H_2 are listed in Table I. The measured in-plane anisotropy field changes systematically with in-plane AR as expected. For AR<1, the magnetization points along the hard axis corresponding to a negative H_1; while for AR>1, H_1 becomes positive. The out of plane anisotropy field H_2 is dominated by the shape anisotropy of these planar structures and it is only weakly dependent on aspect ratio.

Next, we measure the nonlinear change in the resonance line shape, as in Fig. 1, for each sample at various applied fields. Because we do not know the amplitude of precession, it was only experimentally feasible to determine the sign of the nonlinear coefficient. The spectra were fit to a modified Lorentzian function,

$$L(H_{\rm appl}) = \frac{a}{\left[H_{\rm appl} - H_0 + N' L(H_{\rm appl})\right]^2 / \Delta H^2 + 1} + c(H_{\rm appl} - H_0) + d, \quad (12)$$

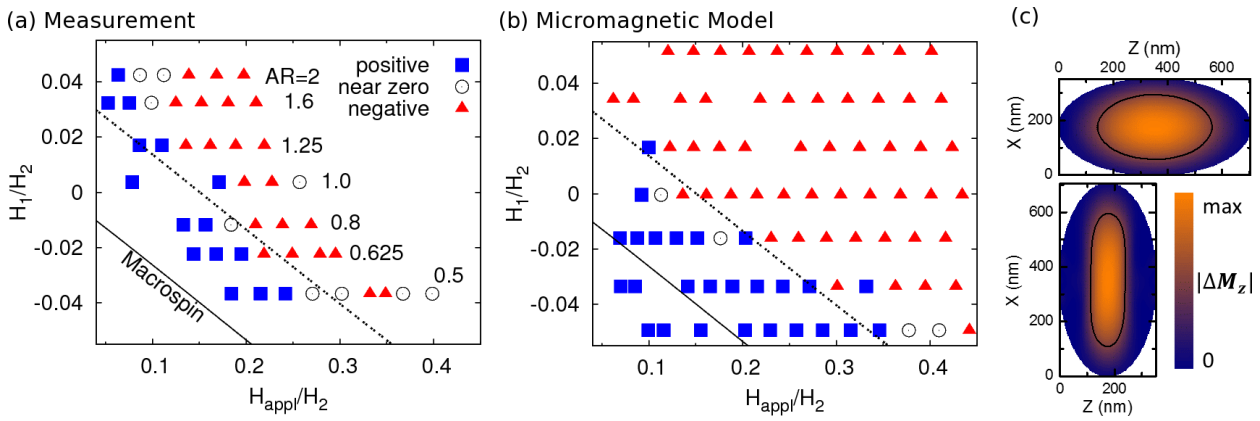

FIG. 4: (Color online) Measured (a) and modeled (b) sign of nonlinear coefficient as a function of normalized in-plane anisotropy field (H_1/H_2) and applied field ($H_{\rm appl}/H_2$). The aspect ratios are labeled for each sample, corresponding to a given anisotropy obtained from ferromagnetic resonance measurements. The "near zero" open circles indicate that the fit value of N' was smaller than its standard deviation. The solid lines in (a) and (b) are the condition for zero nonlinearity predicted by the macro-spin model. The dotted lines are the zero nonlinearity curves from the macro-spin model including the effect of non-uniform magnetization. (c) Modeled precession amplitude profiles ($|\Delta M_z|$) of the main mode for the cases where the field is parallel (top, AR=2) and perpendicular (bottom, AR=0.5) to the long axis of the ellipses. The contour lines mark where $|\Delta M_z|$ is half of its maximum value.

where the small-amplitude resonance field H_0, signal amplitude, a, nonlinear coeffiecient, N', background slope c and background offset d are all fitting parameters. The sign of N' is plotted in Fig. 4(a). The horizontal rows of points correspond to measurements made on single ellipses at different frequencies and resonance fields.

The sign change for the nonlinear coefficient is observed for all 7 samples measured, and the nonlinear coefficient tends to be positive at lower fields and it becomes negative at high fields. The nonlinear coefficient is also sensitive to the in-plane anisotropy field. For a given applied field, the nonlinear coefficient decreases with increasing H_1. The trend of field dependence on the nonlinear coefficient is consistent with the prediction from the macrospin model previously discussed. However, the measured nonlinear coefficient appears to be more positive than that predicted. In other words, the measured zero nonlinear coefficients occur at higher fields than the prediction.

OOMMF[22] micromagnetic modeling is also performed to the investigate the nonlinear

resonance shift. Modeled sample geometries correspond to the designed dimensions of the experimental samples. Material parameters were chosen to mimic Permalloy: $M_s = 800$ kA/m and exchange stiffness $A = 13$ pJ/m, yielding an intrinsic exchange length of 5.69 nm. Cell sizes of both 3 nm x 3 nm x 25 nm and 6 nm x 6 nm x 25 nm were used and no appreciable differences were encountered in the results. Edge corrections were used to mitigate the effects of a the square computational grid[23]. Thermal effects were not modeled.

The computational experiments follow closely the laboratory measurements and analysis methods. An efficient pulse-response method was used to calculate the low-power resonances[24], which were fit to obtain values of the in-plane and out-of-plane anisotropy fields, H_1 and H_2 respectively. Results are listed in Table I. For model particles that approximate the size and shape of the experimental structures, the model yields a slightly broader range of H_1 values and slightly larger values of H_2 than the measurements.

The high-power response was then determined by subjecting the modeling "sample" to an oscillating microwave field with different combinations of microwave frequency, microwave power and static applied field. After integrating the equations of motion over 10 ns, a limit cycle was approached and the magnetization was time-averaged over 5 ns to determine the quasi-static magnetization reduction. To trace out each simulated FMRFM response curve, this process was repeated for different applied fields and the results were fit in the same way as the measured curves.

The model results are shown in Fig. 4(b). In the measured and modeled results, a few of the points appear to be missing. These points correspond to situations where more complex line shapes were observed, presumably due to nonlinear excitation of multiple modes. In agreement with the experimental results, the modeling yields a similar dependence of H_1 and H_{appl}. More importantly, we point out that the micromagnetic modeling also exhibits an offset in the nonlinear coefficient compared to the macrospin result. With a given H_1, the modeled applied field for zero nonlinearity is higher than that predicted by the macrospin theory, Eq. (8).

We now propose a possible origin of the difference between the macro-spin prediction of the zero nonlinearity condition and the experimental and micromagnetic results. The offset in the measured nonlinear coefficient can be understood as a nonlinear magnetostatic mechanism arising from the non-uniformity of the precession in the excited mode. FMR precession modes in the confined structures are highly non-uniform, as exemplified in Fig. 4(c).

Thus, the time-average static magnetization, $\langle M_z \rangle$, is also non-uniform. For example, the dark regions at the edges in Fig. 4(c) represent zero precession where $\langle M_z \rangle \approx M_s$ and in the bright regions near the structure center the precession amplitude reaches maximum with reduced $\langle M_z \rangle < M_s$.

As a consequence, the spatial variation of $\langle M_z \rangle$ results in an additional demagnetizing field, ΔH_d, with a component parallel to the applied field and a spatial dependence that is related to the precession pattern of the excited mode. This additional demagnetizing field is the change in the demagnetizing field due to the precession-induced change in the quasi-static magnetization, $\Delta M_z(\vec{r'})$:

$$\Delta H_d(\vec{r}) = -\frac{1}{4\pi} \int d^3\vec{r'} \, \frac{d}{dz'} \langle \Delta M_z(\vec{r'}) \rangle \frac{\vec{r} - \vec{r'}}{|\vec{r} - \vec{r'}|^3} \tag{13}$$

With zero precession amplitude, $\langle \Delta M_z \rangle$ is zero and hence $\Delta H_d = 0$, but ΔH_d grows with increasing precession amplitude. Since ΔH_d is roughly aligned with H_{appl}, a lower applied field is required to reach the resonance at a higher microwave power. This explains why the resonance field tends to "fold over" toward low field direction for our nanostructures, or equivalently, the nonlinear coefficient measured in the nanostructures tends to be more positive than that predicted by the macrospin.

In eq. (13), we have related a dynamics-induced change in the magnetization to a change in the magnetostatic field. We therefore define a nonlinear, mode dependent shift in the demagnetization parameter,

$$\Delta N_z = -\frac{\int d\vec{r} \, \Delta H_d(\vec{r})}{\int d\vec{r} \, \langle \Delta M_z(\vec{r}) \rangle}. \tag{14}$$

For nonlinear effects, the nonuniformity essentially shifts the in-plane anisotropy field H_1 by $\Delta H_1 = -\Delta N_z M_s$, or, since $H_2 \gg H_1$,

$$\frac{\Delta H_1}{H_2} \approx -\Delta N_z. \tag{15}$$

We use the modeled precession mode profile of AR = 0.5 sample in Fig. 4(c) (bottom) to calculate ΔH_d, and we compute $\Delta H_1 / H_2 \approx 0.04$. The dotted lines in Fig. 4 include the estimation of magnetization non-uniformity effect. They show good agreement with the experimental and micromagnetic results.

In a separate study, the influence of the shape confinement on the nonlinear coefficient is also investigated in the perpendicular geometry. de Loubens and colleagues have experimentally studied the out-of-plane magnetized disks, and they found the non-uniform

magnetization also significantly enhances the nonlinear coefficient in that configuration.[25] At much higher driving fields where the nonlinear frequency shifts are on the order of 1 GHz, hybridization of the normal modes has been observed with qualitative changes in the mode profiles.[26]

In conclusion, we have shown the nonlinear resonance shift in patterned nanostructures. The measured nonlinear coefficient can be either positive or negative depending on the applied field and the anisotropy fields. A classical macro-spin approach has been used to demonstrate the sign of the nonlinear coefficient is determined by the field configuration (H_{appl} and H_1), through the details of precession orbits. The nonlinear coefficients measured from a set of elliptical samples are consistent with the results from the macro-spin analysis and micromagnetic modeling. However, both the measurements and the modeling of the confined structures indicate nonlinear coefficients that are more positive than the macro-spin analysis. We explain that this substantial offset in the nonlinear coefficient is due to the non-uniform precession mode in the confined structures via a magnetostatic mechanism.

We thank G. de Loubens and O. Klein for useful discussions. Dr. Guo acknowledges support under the Cooperative Research Agreement between the University of Maryland and the National Institute of Standards and Technology Center for Nanoscale Science and Technology, Award 70NANB10H193, through the University of Maryland. Dr. Belova acknowledges support from the Swedish Research Council and the Carl Tryggers Research Foundation.

---

* Electronic address: `feng.guo@nist.gov`

† Electronic address: `robert.mcmichael@nist.gov`

[1] P. E. Wigen, ed., *Nonlinear Phenomena and Chaos in Magnetic Materials* (World Scientific, 1994).

[2] A. G. Gurevich and G. A. Melkov, *Magnetization Oscillations and Waves* (CRC Press, Inc., 1996), chap. 9 & 10.

[3] D. D. Stancil and A. Prabhakar, *Spin Waves, Theory and Applications* (Springer, 2010), chap. 9.

[4] H. Suhl, J. Phys. Chem. Solids **1**, 209 (1957).

[5] R. D. McMichael and P. E. Wigen, Phys. Rev. Lett. **64**, 64 (1990).

[6] S. O. Demokritov, V. E. Demidov, O. Dzyapko, G. A. Melkov, A. A. Serga, B. Hillebrands, and A. N. Slavin, Nature **443**, 430 (2006).

[7] Y. S. Gui, A. Wirthmann, N. Mecking, and C.-M. Hu, Phys. Rev. B **80**, 060402 (2009).

[8] M. P. Wismayer, B. W. Southern, X. L. Fan, Y. S. Gui, C.-M. Hu, and R. E. Camley, Phys. Rev. B **85**, 064411 (2012).

[9] T. Gerrits, P. Krivosik, M. L. Schneider, C. E. Patton, and T. J. Silva, Phys. Rev. Lett. **98**, 207602 (2007).

[10] Y. Khivintsev, B. Kuanr, T. J. Fal, M. Haftel, R. E. Camley, Z. Celinski, and D. L. Mills, Phys. Rev. B **81**, 054436 (2010).

[11] V. E. Demidov, H. Ulrichs, S. O. Demokritov, and S. Urazhdin, Phys. Rev. B **83**, 020404 (2011).

[12] A. Slavin and V. Tiberkevich, IEEE Trans. Mag. **45**, 1875 (2009).

[13] V. Tiberkevich, I. Krivorotov, G. Gerhart, and A. Slavin, J. Magn. Magn. Mater. **321**, L53 (2009).

[14] V. V. Naletov, G. de Loubens, G. Albuquerque, S. Borlenghi, V. Cros, G. Faini, J. Grollier, H. Hurdequint, N. Locatelli, B. Pigeau, et al., Phys. Rev. B **84**, 224423 (2011).

[15] H.-J. Chia, F. Guo, L. M. Belova, and R. D. McMichael, Applied Physics Letters **101** (2012).

[16] A. Hamadeh, G. de Loubens, V. V. Naletov, J. Grollier, C. Ulysse, V. Cros, and O. Klein, Phys. Rev. B **85**, 140408 (2012).

[17] I. Lee, Y. Obukhov, G. Xiang, A. Hauser, F. Yang, P. Banerjee, D. Pelekhov, and P. Hammel, Nature **466**, 845 (2010).

[18] H.-J. Chia, F. Guo, L. M. Belova, and R. D. McMichael, Phys. Rev. Lett. **108**, 087206 (2012).

[19] R. Adur, C. Du, H. Wang, S. A. Manuilov, V. P. Bhallamudi, C. Zhang, D. V. Pelekhov, F. Yang, and P. C. Hammel (2014), arXiv:1405.4203.

[20] F. Guo, L. M. Belova, and R. D. McMichael, Phys. Rev. Lett. **110**, 017601 (2013).

[21] L. M. Belova, E. D. Dahlberg, A. Riazanova, J. J. L. Mulders, C. Christophersen, and J. Eckert, Nanotechnology **22**, 145305 (2011).

[22] M. J. Donahue and D. G. Porter, in *Interagency Report NISTIR 6376* (National Institute of Standards and Technology, Gaithersburg, MD, 1999).

[23] M. J. Donahue and R. D. McMichael, IEEE Trans. Mag. **43**, 2878 (2007).

[24] R. D. McMichael and M. D. Stiles, J. Appl. Phys **97**, 10J901 (2005).

[25] G. de Loubens and O. Klein, private communication (2014).

[26] V. E. Demidov, M. Buchmeier, K. Rott, P. Krzysteczko, J. Münchenberger, G. Reiss, and S. O. Demokritov, Phys. Rev. Lett. **104**, 217203 (2010).